Single-cell Analysis: Visualizing Pharmaceutical and Metabolite Uptake in Cells with Label-free 3D Mass Spectrometry Imaging

Melissa K. Passarelli,[*,†] Carla F. Newman,[*,‡] Peter S. Marshall,[‡] Andrew West,[‡] Ian S. Gilmore,[†,¶] Josephine Bunch,[†,¶] Morgan R. Alexander,[¶] and Colin T. Dollery[‡]

National Centre of Excellence in Mass Spectrometry Imaging (NiCE-MSI), National Physical Laboratory (NPL), Teddington, Middlesex, TW11 0LW, U.K., GlaxoSmithKline, Stevenage, UK., and Univerity of Nottingham, School of Pharmacy University Park, Nottingham, NG7 2RD, U.K.

E-mail: melissa.passarelli@npl.co.uk; carla.f.newman@gsk.com

Abstract

Detecting metabolites and parent compound within a cell type is now a priority for pharmaceutical development. In this context, three-dimensional secondary ion mass spectrometry (SIMS) imaging was used to investigate the cellular uptake of the antiarrhythmic agent amiodarone, a phospholipidosis-inducing pharmaceutical compound. The high lateral resolution and 3D imaging capabilities of SIMS combined with the multiplex capabilities of ToF mass spectrometric detection allows for the visualization of pharmaceutical compound and metabolites in single cells. The intact, unlabeled drug compound was successfully detected at

[*]To whom correspondence should be addressed
[†]National Physical Laboratory
[‡]GlaxoSmithKline
[¶]University of Nottingham

therapeutic dosages in macrophages (cell line: NR8383). Chemical information from endogenous biomolecules was used to correlate drug distributions with morphological features. From this spatial analysis, amiodarone was detected throughout the cell with the majority of the compound found in the membrane and subsurface regions and absent in the nuclear regions. Similar results were obtained when the macrophages were doped with amiodarone metabolite, desethylamiodarone. The FWHM lateral resolution measured across an intracellular interface in a high lateral resolution ion images was approximately 550 nm. Overall, this approach provides the basis for studying cellular uptake of pharmaceutical compounds and their metabolites on the single cell level.

In pharmacology, it is often assumed that the drug concentration at the effector site is equivalent to the serum concentration.[1] However, this is often not the case, as factors such as cellular uptake, sequestering and accumulation can affect the amount of drug that reaches the target site and skews the dose-response dynamic. In a recent review,[2] it is highlighted "that many drug targets are intracellular...[and therefore] to predict the pharmacological effect accurately, there must be data concerning the concentration at the target" and that "knowledge of the drug concentration at its site of action within cells is becoming increasingly important in pharmacology and therapeutics." Consequently, the ability to analyze drug compounds in the complex cellular environments is a priority for modern pharmaceutical research. Indeed, evaluating drug uptake on the single cell level would provide new opportunities in drug development by evaluating more precisely the dose-response behavior of individual cells.

Mass spectrometry imaging (MSI) techniques are well-suited for analyzing drug distributions in biological materials. The method has the advantage of being label-free and capable of multiplexed analyzes when coupled to a ToF mass analyzer. The parallel detection of the drug compound and the local endogenous chemistry permits the correlation of drug distributions with respect to morphological features. MALDI and DESI are currently the main MSI methodologies used by pharmaceutical companies, these methods have been successfully employed to investigate drug distributions in tissues.[3–6] Unfortunately these methods do not have the lateral resolution to

achieve sub-micrometer imaging, however, it is worth noting that recent technological advances in the field of MALDI has improved the lateral resolution to a few micrometers, thus allowing the visualization of large cells and organelles.[7–9]

In this context, 3D ToF-SIMS imaging is a potentially powerful analytical platform for the pharmaceutical industry. SIMS has been successfully applied to investigating drug distribution in medical devices[10] and various drug delivery systems.[11,12] The sub-micron lateral resolution and nanometer depth resolution of SIMS opens the possibility for three-dimensional molecular imaging of pharmaceuticals at the single cell level.[13–17] Although, sensitivity and matrix effects have limited the role of SIMS in pharmacology, technological advancements, particularly the advent of cluster ion sources, have improved the technique's sensitivity.[18,19] The advantage of cluster sources is two-fold; as an analysis beam cluster sources improve molecular ion yields and as a sputtering beam, they reduce damage accumulation allowing the molecular ion sensitivity to be maintained throughout the sample. With these advances, as demonstrated here, the use of SIMS in the analysis of pharmaceutical compounds and their metabolites in single cell is now achievable.

In this report, 3D ToF-SIMS imaging was used to successfully detect the anti arrhythmia drug compound amiodarone and its metabolite, desethylamiodarone, in single macrophages. The intact molecular ion of the target drug compound amiodarone, m/z 646.0, was detected throughout the cell. The majority of the compound signal was observed in the surface and subsurface regions of the cell. Although the molecular ion signal intensity dissipates with depth, the signal of the molecular ion is still observed above a signal-to-noise (S/N) level of 3 throughout the analysis. Overall, this study demonstrates the potential of ToF-SIMS as a bio-analytical method for the analysis of cellular uptake of drugs and metabolite at the single cell level.

Experimental Methods

Cell culture. NR8383 cells, an immortalized cell line derived from a lung macrophage (Sprague-Dawley rat), were grown on Nunc Lab-Tek II Chamber slides (Thermo Scientific, USA) with

Ham's F-12 Nutrient Mixture medium containing GlutaMax and Phenol Red (Gibco, USA) and 15 % dialyzed, heat-inactivated fetal bovine serum (Gibco, USA). 5 mg/mL stock solutions of amiodarone hydrocholoride (Sigma-Aldrich, CAS 19774-82-4, purity $\geq$ 98 %) and *N*-desethylamiodarone hydrochloride solution (Sigma-Aldrich, CAS 96027-74-6) were prepared in 50:50 water/ MeOH. The stock solutions were added to the growth medium for a final medium concentration of 1.56 μg/mL. The cells were incubated (5 % CO_2 and 37 °C) in the drug or metabolite doped medium solution for 72 hrs. Control cells were incubated alongside the doped cells.

Freeze-drying procedure. The medium was removed and the cells were washed three times with 150 mM ammonium formate solution (pH-balanced, Sigma-Aldrich, USA).[20] Excess liquid was removed and the cells were frozen using a CoolSink XT 96F plate (BioCision, USA) at -80 °C. The frozen cells were dried under vacuum in a miVac with SpeedTrap (Genevac, USA) for approximately 1 hour. The samples were stored at -80 °C. Before ToF-SIMS analysis the samples were warmed to room temperature in a vacuum chamber.

Instrumentation. ToF-SIMS analyses were performed on a TOF-SIMS IV mass spectrometer (ION-TOF GmbH, Münster, Germany). The dual beam experiment used a 25 keV Bi_3^+ primary ion beam for imaging and a 20 keV Ar_{2000}^+ beam for sputtering. The bismuth ion source was operated using two imaging mode; the high current, high mass resolution mode and the high lateral resolution mode.

High mass resolution ion images were collected over a surface area of 125 μm x 125 μm using a pulsed analysis beam (pulse width = 23 ns, mass resolution (m/Δm) at m/z 646 $\sim$3400). At 256 x 256 pixels per image, the pixel width was 0.5 μm. Each image was obtained with a final ion dose of 2.2 x 10^{12} primary ions/cm^2. The dose was kept below the static limit of the 10^{13} primary ions/cm^2 to minimize surface damage. After recording each image, the sample was eroded with a sputter beam with an Ar_{2000}^+ ion dose of 3.7 x 10^{13} ions/cm^2 over an area 250 μm x 250 μm. The total acquisition time for each 3D image was approximately 2 hrs. Data was collected in the positive secondary ion mode.

High lateral resolution ion images were collected over a surface area of 50 μm x 50 μm using

a pulsed analysis beam (pulse width = 100 ns, mass resolution (m/Δm) at m/z 127 $\sim$ 335). At 256 x 256 pixels per image, the pixel width was 0.2 μm. Each image was obtained with a final ion dose of 6.5 x 10^{11} primary ions/cm^2. After recording each image, the sample was eroded with a sputter beam with an Ar^+_{2000} ion dose of 3.9 x 10^{13} ions/cm^2.

All image analyzes were performed using ION-TOF SurfaceLab (Version 6.3, ION-TOF, Münster, Germany) and MATLAB 2014a. Individual cells were outlined with a polyline tool using the total ion count image and pixels above the threshold (25% of the total ion counts) were selected as regions of interest (ROI). Chemical structures were drawn in ChemDraw 14.0. The high lateral resolution imaging experiments were collected in the negative secondary ion mode. Image lateral resolution measurement were obtained by plotting the ion intensities for the various analytes across an intracellular features. The linescans were fitted with a error function and the FWHM lateral resolution was measured.[21,22]

Results and Discussion

Amiodarone [KEGG drug: D02910] is an effective Vaughan-Williams class III antiarrhythmic medication (potassium channel blocker) known to delay repolarization in the smooth muscle cell in the heart, resulting in heartbeats with prolonged action potential durations and refractory periods.[23] Unfortunately, the therapeutic value of amiodarone is diminished by adverse and potentially dangerous side effects.[24] In clinical studies, the concentration of amiodarone in serum was correlated to therapeutic and toxic effects in patents.[25] For patients with amiodarone serum concentrations below 1 μg/mL, the effectiveness of the drug as an anti-arrhythmia agent was reduced. While, patients with amiodarone serum concentrations above 2.5 μg/mL often experience adverse reactions. Long-term usages of amiodarone leads to drug induced phospholipidosis, a lysosomal storage disorder characterized by the prevalence of "foamy" or lipid-laden macrophages.

Although the link between foamy macrophages and drug-induced toxicity is unclear, the impairment of cellular functions and the accumulation for lipids in macrophages has been the subject

of numerous investigated.[26–29] Amiodarone is a cationic amphiphilic drug whose hydrophobic domain allows it to cross the lipid membrane, including that of the lysosome. Inside the acidic environment of the lysosome, amiodarone is hydrolyzed.[28] It is speculated that the drug accumulates in the lysosome, as it is unable to re-cross the membrane in the hydrolyzed state, and inhibits the degradation of phospholipase A, a protein responsible for lipid catabolism.[29] As a result, phospholipids and drug accumulate in the lysosomes and impairs cellular functions. Although the inhibition of late stage endosomal processes has been shown to suppresses virus activation[30] (*e.g.* SARS), a attribute that may broaden the therapeutic application of amiodarone, without a clear understanding of the drug's role in organ-based toxicity, the therapeutic value of amiodarone is limited.

Lipid accumulations in foamy macrophages are visible with histological staining and light microscopy and are also detected as lamellar inclusion bodies with electron microscopy. It is important to note, that these detection methods do not provide information on the presence of the drug, but only detect the morphological changes caused by the drug. Therefore, a method, such as SIMS, with the ability to directly detect the drug compound inside individual cell may provide clues as to its potential toxicity.

In this investigation, the intact protonated molecule, $[M+H]^+$, of the drug compound amiodarone, $C_{25}H_{29}I_2NO_3$, was detected at m/z 646.0 in the drug-doped lyophilized macrophages (see Figure 1A). The peak and isotope pattern was in agreement with the reference spectrum and theoretical isotope pattern for amiodarone (see Supporting Information, Figure-S1). A peak at m/z 520.1 was also detected and identified as protonated amiodarone with a missing iodine, $[C_{25}H_{30}INO_3+H]^+$. The peak at m/z 520.1 was also present in the reference spectrum.

The total ion contribution for the amiodarone related peaks at m/z 646.0 and m/z 520.1, displayed in Figure 1B, shows that amiodarone is localized within the cells. The distribution of amiodarone across the cell appears to be relatively uniform, except in the region indicated with the white arrow. The absence of amiodarone signal in this region is made clear when we examined the endogenous species in this region. This region is occupied by a number of known nuclear

markers, including the molecular ion of adenine, a purine nucleobase, at m/z 136.1 and a fragment of ribose, $C_5H_5O^+$ at m/z 81,[31,32] the sugar functional group that makes up the backbone of RNA and DNA. Additional oxygenated hydrocarbon species, including $C_5H_6O_2{}^+$ at m/z 98.0, $C_4H_4O^+$ at m/z 68.0 and $C_3H_4O^+$ at m/z 56.0 also co-localized to the nucleus. The cell nucleus was unequivocally identified using the chemical cues from the mass spectrum and as expected, the drug compound is not observed in this region of the cell. The phosphocholine fragment (m/z 184), ribose fragment (m/z 81) and amiodarone (m/z 646) ion intensities across the large cell, defined as ROI 1, is shown in Figure 1E. The intracellular interface between the ribose and drug signal was fitted with a error function (erf). Assuming that the lateral resolution is limited by the diameter of the Gaussian -shaped ion beam, the full width half maximum (FWHM) lateral resolution, which is equivalent to 2.3548 times the standard deviation, σ, was calculated to be 3.4 μm.

In Figure 1C, we also mapped endogenous species that co-localize with the drug compound, including phosphocholine fragment species $C_5H_{12}N^+$ at m/z 86.1, $C_5H_{12}N^+$ at m/z 104.1, $C_2H_6O_4P^+$ at m/z 125.0, $C_5H_{13}NO_3P^+$ at m/z 166.1, $C_5H_{15}NO_4P^+$ at m/z 184.1 and $C_8H_{19}NO_4P^+$ at m/z 224.1.[33] The co-localization of amiodarone and lipid was expected. Amiodarone is extremely lipophilic (log $P_{oil/water}$ = 6.3).[34] The high propensity of amiodarone to accumulate in lipid-rich regions contributes to its therapeutic properties as well as its adverse side effects. In a cardiac cell, the incorporation of amiodarone into the cell membrane perturbs the properties of the phospholipid bilayer structure and contributes to its antiarrhythmic abilities.[35]

Table 1: For the individual cells defined in the ion image in Figure 1C, the percent area of coverage, average amiodarone counts per pixel summed across the depth scale and cell diameters were calculated. The average amiodarone count per pixel was calculated by dividing the background-subtracted intensity of the peak at m/z 646.0 summed over the ROI by the total number of pixels in the selected ROI.

	ROI 1	ROI 2	ROI 3	ROI 4
Area (%)	9.82	3.25	5.79	2.55
Counts per pixel	8.5	2.7	3.3	2.4
Diameter (μm)	45	26	33	22

Variations in the morphology of the cell and relative cellular amiodarone ion signal intensity

was observed throughout the population. Immortalized cell lines are typically considered to have relatively homogeneous properties; however, cell-to-cell variations are expected. The SIMS image was divided into four ROI and the chemical signature was examined for each cell (see Figure 1 D). The approximate size and counts per pixel for the signal intensity of amiodarone for each cell is reported in Table 1. The cells in ROI 3 and 4 are physically attached so the boundary was approximated. The cell in ROI 1 is significantly larger and has relatively more intense amiodarone signal (m/z 646.0) than the other cells in the ion image. The cell is potentially "foamy" and accumulating lipid and drug. The cell in ROI 3 is most likely in the process of division, nuclear material is localized in two regions of the cell and the cell is slightly larger than the cells defined in ROI 2 and 4.

With 3D ToF-SIMS imaging, the distribution of the drug and endogenous species are collected as a function of depth. After the surface of the cells was sputtered away, the drug compound (green) can be seen inside the cell (see Figure 2). Ion image at selected sputter cycles throughout are displayed in Figure 3. For clarity, the ion image acquired before the first sputter cycle was not included. The molecular ion peak of amiodarone was detected throughout the cell with the majority of the compound signal observed in the surface and subsurface regions. Although the molecular ion signal intensity diminished with depth, the signal of the molecular ion is still observed at a S/N level above 3 throughout the analysis (see Figure 3 D and Table 2). It should be noted that the high surface amiodarone signal intensity is most likely a result of the sample preparation method used in this study and does not reflect an equilibrium state in culture. For more accurate intracellular distributions, cryogenic sample preparation methods are required. Here, for the purposes of showing the efficacy of detecting drug uptake at the single cell level and therapeutic doses, the cells were freeze-dried.

The presence of the drug compound deep inside the cell, as shown in Figure 3, is clear evidence of cellular uptake. This observation is supported by conventional radio-labeling studies preformed by Stadler and co-workers.[30] Through the systematic inhibition of the endocytotic pathways (*i.e.* clathrin-mediated, caveolae-mediated, phagocytosis) studies show that amiodarone does not have

Table 2: The signal-to-noise (S/N) and maximum count (MC) for the molecular ion of the drug compound for various sputter cycles throughout the cell in Figure 1 defined by ROI 1 are provided.

Dose (ions/cm^2)	cycle number	S/N	MC
7.4-18.5 x 10^{13}	2-5	81.7	1550
1.85-3.7 x 10^{14}	5-10	67.88	1100
3.7-5.6 x 10^{14}	10-15	33.71	480
5.6-7.4 x 10^{14}	15-20	22.85	221
7.4-9.3 x 10^{14}	20-25	15.8	124
0.9-1.1 x 10^{15}	25-30	11.2	92
1.1-1.3 x 10^{15}	30-35	8.9	50
1.3-1.5 x 10^{15}	35-40	7.6	36

a preferred endocytotic pathway, it is internalized through various methods and routes.[30] Unfortunately, since the quantity of the radiation released by radio-isotope is independent of the structure of the tracer molecule, it is impossible to differentiate the drug molecule from its metabolites. Therefore, the use of radioactive isotopic labels is further complicated by the tracer's potential to change the metabolic pathway and cellular damages from the emission of radio-active beta particles.[36] The direct *in situ* detection of the drug and its metabolites with SIMS, eliminates the need for isotopic labels.

We evaluated the efficacy of SIMS in the detection of desethylamiodarone, the main metabolite of amiodarone. Amiodarone is metabolized by the cytochrome P450 (CYP450) enzymes, specifically cytochrome P450 isoform CYP3A4[37] and CYP2C8[38] in the liver. Since the cell line does not metabolize amiodarone, the lung macrophages were doped with desethylamiodarone.[37,39] The metabolite has also been shown to accumulate in lung macrophages and contribute to the toxic effect of the drug.[40] The SIMS image shows the protonated molecule of the metabolite, $[(C_{23}H_{25}I_2NO_3)+H]^+$, which was detected at m/z 618.0 (see Figure 4). The cellular localization exhibited by the metabolite was similar to its precursor; it was co-localized with the lipid through the cell and absent in the nucleus. In Figure 4A, the cluster of cells in the center of the ion image have a higher count per pixel intensity of the metabolite peak, suggesting accumulation.

High lateral resolution ion image of a cell doped with the amiodarone metabolite, desethylamiodarone, are shown in Figure 5A. In the ion image, the iodine signal, I^-, at m/z 127 (green)

was found throughout the cell, but was absent in the nuclear regions (red). The distribution was consistent with the high mass resolution experiments for both amiodarone and desthlamiodarone. In the negative ion mode, adenine ($C_5H_4N_5^-$) at m/z 134.1 and two phosphate-oxygen fragments, $HP_2O_6^-$ at m/z 158.9 and $NaP_2O_6^-$ at m/z 180.9, were used as nuclear markers. The nuclear morphology, elucidated in the 3D isosurface rendering in Figure 5B, provides a clear intercellular interface to measure the image resolution. A linescan across the nucleus-drug interface was fitted with a *erf* (black) and the FWHM lateral resolution was measured to be 550 nm. In the high lateral resolution imaging mode, the limited ion beam current and long pulse duration reduced the quality of the mass spectral data. As a result, only the iodine in the analyte molecule was present at a sufficient intensity to map its distribution. In present ToF-SIMS instruments, the loss of chemical specificity associated with high lateral resolution imaging experiments prevents its use in animal studies. Since both the drug and metabolite has an iodine group, the two compounds would not be distinguishable when analyzing excised tissue from an animal model. In the NR8383 model system, as previously mentioned, the cell line is unable to metabolize the compound, therefore, we are confident that the iodine signal is from the dosed analyte.

Amiodarone has several advantageous properties that make it ideal for mass spectrometry analyzes, particularly ToF-SIMS. The drug compound has two iodine functional groups. Iodine has the largest mass defect of all the elements; the exact mass of the mono-isotope is 126.9044,[41] which is approximately -753 ppm deviation from the nominal mass. These functional group shift the drug peak to a lower mass-to-charge than the isobaric hydrocarbon-containing species, reducing the potential for spectral interference with endogenous biomolecules. It is also fortunate that this particular drug compound falls within a relatively quiet region of the mass spectrum; clear from the phospholipid region and from sterols and diacylgylcerides species.[33] Also, the tertiary amine in the di-ethylamine moiety, which is reduced to a secondary amine group when metabolized, most likely stabilizes the positively charged species in the gas phase, improving its secondary ion yields compared to the metabolite.

In this case, the chemical features of amiodarone, as described in the supporting information,

facilitated the detection and identification of the compound inside the cells. However, this is often not the case. A significant proportion of pharmaceuticals are small organic molecules that fall within congested regions of the mass spectrum and experience isotopic interference. The MALDI community has employed the high mass resolution of FT-based detection schemes to overcome isobaric interference to image drugs in tissues.[42,43] Efforts are currently underway to incorporate this technology into SIMS instrumentation.[44] New instrumental developments will help to expand the use of SIMS in pharmaceutical applications.

Overall, we have shown that 3D-ToF SIMS provides important pharmacokinetic information on the distribution of drugs and metabolites in single cells. Chemical cues from endogenous species were used to identify and correlate the location of large organelles with the distribution of the drug compound. On the single cell level, variations in the cell size, cell cycle stage and the relative amount of drug compound were observed. 3D imaging of pharmaceutical distributions on the single cell level is an exciting new application for SIMS and the amiodarone-macrophages system is a potential model for future pharmaceutical applications.

Acknowledgement

The authors thank Dr. Dave Hassall and Dr. Andy Nichols of GlaxoSmithKline for discussions on the experimental design of the amiodarone and NR8383 study. We also thank Dr. Alex Shard for his discussion and comments on this manuscript. This work was funded by the 3D nanoSIMS project in the strategic capabilities program of the National Measurement System of the UK Department of Business, Innovation and Skills and by the National Centre for replacement, Refinement and Reduction of Animals in Research (NC3Rs) NC/C013110/1.

Contributions: Performed biological research: CFN; Performed SIMS research: MKP, CFN; Analyzed data and wrote the paper: MKP; initial design: JB, PSM; Academic advisor to CFN: MA; Direction: CTD, AW, ISG; Funding: JB, ISG.

Notes and References

(1) Plomp, T.; Van Rossum, J.; Robles, d. M. E.; Van Lier, T.; Maes, R. *Drug. Res.* **1983,** *34,* 513–520.

(2) Dollery, C. *Clin. Pharmacol. Ther.* **2012,** *93,* 263–266.

(3) Greer, T.; Sturm, R.; Li, L. *J. Proteomics* **2011,** *74,* 2617–2631.

(4) Rubakhin, S. S.; Jurchen, J. C.; Monroe, E. B.; Sweedler, J. V. *Drug Discov. Today* **2005,** *10,* 823–837.

(5) Prideaux, B.; Stoeckli, M. *J. Proteomics* **2012,** *75,* 4999–5013.

(6) Nilsson, A.; Goodwin, R. J.; Shariatgorji, M.; Vallianatou, T.; Webborn, P. J.; Andrén, P. E. *Anal. Chem.* **2014,** .

(7) Spengler, B.; Hubert, M. *J. Am. Soc. Mass Spectrom.* **2002,** *13,* 735–748.

(8) Schober, Y.; Guenther, S.; Spengler, B.; RoÌĹmpp, A. *Anal. chem.* **2012,** *84,* 6293–6297.

(9) Zavalin, A.; Todd, E. M.; Rawhouser, P. D.; Yang, J.; Norris, J. L.; Caprioli, R. M. *J. Mass Spectrom.* **2012,** *47,* 1473–1481.

(10) Fisher, G. L.; Belu, A. M.; Mahoney, C. M.; Wormuth, K.; Sanada, N. *Anal. Chem.* **2009,** *81,* 9930–9940.

(11) Belu, A.; Mahoney, C.; Wormuth, K. *J. Control. Release* **2008,** *126,* 111–121.

(12) John, C.; Odom, R.; Salvati, L.; Annapragada, A.; Lu, M. F. *Anal. Chem* **1995,** *67,* 3871–3878.

(13) Trouillon, R.; Passarelli, M. K.; Wang, J.; Kurczy, M. E.; Ewing, A. G. *Anal. Chem* **2012,** *85,* 522–542.

(14) Passarelli, M. K.; Ewing, A. G. *Curr. Opin. Chem. Biol.* **2013,** *17,* 854–859.

(15) Gilmore, I. S. *JVST A* **2013,** *31,* 050819.

(16) Passarelli, M. K.; Ewing, A. G.; Winograd, N. *Anal. Chem* **2013,** *85,* 2231–2238.

(17) Fletcher, J. S.; Rabbani, S.; Henderson, A.; Blenkinsopp, P.; Thompson, S. P.; Lockyer, N. P.; Vickerman, J. C. *Anal. chem.* **2008,** *80,* 9058–9064.

(18) Winograd, N. *Anal. Chem.* **2005,** *77,* 142–A.

(19) Winograd, N. *Anal. Chem.* **2014,** *87,* 328–333.

(20) Nygren, H.; Eriksson, C.; Malmberg, P.; Sahlin, H.; Carlsson, L.; Lausmaa, J.; Sjövall, P. *Colloids Surf., B* **2003,** *30,* 87–92.

(21) Seah, M. *Surf. Interface Anal.* **2002,** *33,* 950–953.

(22) Passarelli, M. K.; Wang, J.; Mohammadi, A. S.; Trouillon, R.; Gilmore, I.; Ewing, A. G. *Anal. chem.* **2014,** *86,* 9473–9480.

(23) Papiris, S. A.; Triantafillidou, C.; Kolilekas, L.; Markoulaki, D.; Manali, E. D. *Drug Saf.* .

(24) Dusman, R. E.; Stanton, M. S.; Miles, W. M.; Klein, L. S.; Zipes, D. P.; Fineberg, N. S.; Heger, J. J. *Circulation* **1990,** *82,* 51–59.

(25) Rotmensch, H. H.; Belhassen, B.; Swanson, B. N.; Shoshani, D.; Spielman, S. R.; Greenspon, A. J.; Grenspan, A. M.; Vlasses, P. H.; Horowitz, L. N. *Ann. Intern. Med.* **1984,** *101,* 462–469.

(26) Anderson, N.; Borlak, J. *FEBS Lett.* **2006,** *580,* 5533–5540.

(27) Mesens, N.; Desmidt, M.; Verheyen, G. R.; Starckx, S.; Damsch, S.; De Vries, R.; Verhemeldonck, M.; Van Gompel, J.; Lampo, A.; Lammens, L. *Toxicol. Pathol.* **2012,** *40,* 491–503.

(28) Reasor, M. J.; Ogle, C. L.; Miles, P. R. *Exp Lung Res* **1990,** *16,* 577–591.

(29) Abe, A.; Shayman, J. A. *J. Lipid Res.* **2009,** *50,* 2027–2035.

(30) Stadler, K.; Ha, H. R.; Ciminale, V.; Spirli, C.; Saletti, G.; Schiavon, M.; Bruttomesso, D.; Bigler, L.; Follath, F.; Pettenazzo, A.; Baritussio, A. *Am. J. Respir. Cell Mol. Biol.* **2008,** *39,* 142–149.

(31) Rao, A. N.; Vandencasteele, N.; Gamble, L. J.; Grainger, D. W. *Anal. chem.* **2012,** *84,* 10628.

(32) Tyler, B. J. *TOF-SIMS: Materials Analysis by Mass Spectrometry* **2013,** 485.

(33) Passarelli, M. K.; Winograd, N. *BBA- Mol.Cell Biol. L.* **2011,** *1811,* 976–990.

(34) Trumbore, M.; Chester, D.; Moring, J.; Rhodes, D.; Herbette, L. *Biophys. J.* **1988,** *54,* 535–543.

(35) Maresova, L.; Muend, S.; Zhang, Y.-Q.; Sychrova, H.; Rao, R. *J. Biol Chem.* **2009,** *284,* 2795–2802.

(36) Hu, V. W.; Heikka, D. S.; Dieffenbach, P. B.; Ha, L. *FASEB J.* **2001,** *15,* 1562–1568.

(37) Zahno, A.; Brecht, K.; Morand, R.; Maseneni, S.; Török, M.; Lindinger, P. W.; Krähenbühl, S. *Biochem. Pharmacol.* **2011,** *81,* 432–441.

(38) Ohyama, K.; Nakajima, M.; Nakamura, S.; Shimada, N.; Yamazaki, H.; Yokoi, T. *Drug Metab. Dispos.* **2000,** *28,* 1303–1310.

(39) Ohyama, K.; Nakajima, M.; Suzuki, M.; Shimada, N.; Yamazaki, H.; Yokoi, T. *Br. J. Clin. Pharmacol.* **2000,** *49,* 244–253.

(40) Antonini, J. M.; Reasor, M. J. *Biochem. Pharmacol.* **1991,** *42,* S151–S156.

(41) Lide, D. R. "Handbook of chemistry and physics 95th edition", 2014.

(42) Cornett, D. S.; Frappier, S. L.; Caprioli, R. M. *Anal. Chem.* **2008,** *80,* 5648–5653.

(43) Marko-Varga, G.; Fehniger, T. E.; Rezeli, M.; Döme, B.; Laurell, T.; Végvári, Á. *J. Proteomics* **2011,** *74,* 982–992.

(44) http://www.npl.co.uk/news/3d-nanosims-label-free-molecular-imaging.

Graphical TOC Entry

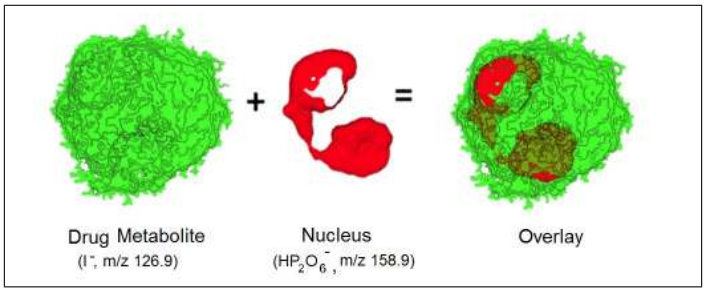

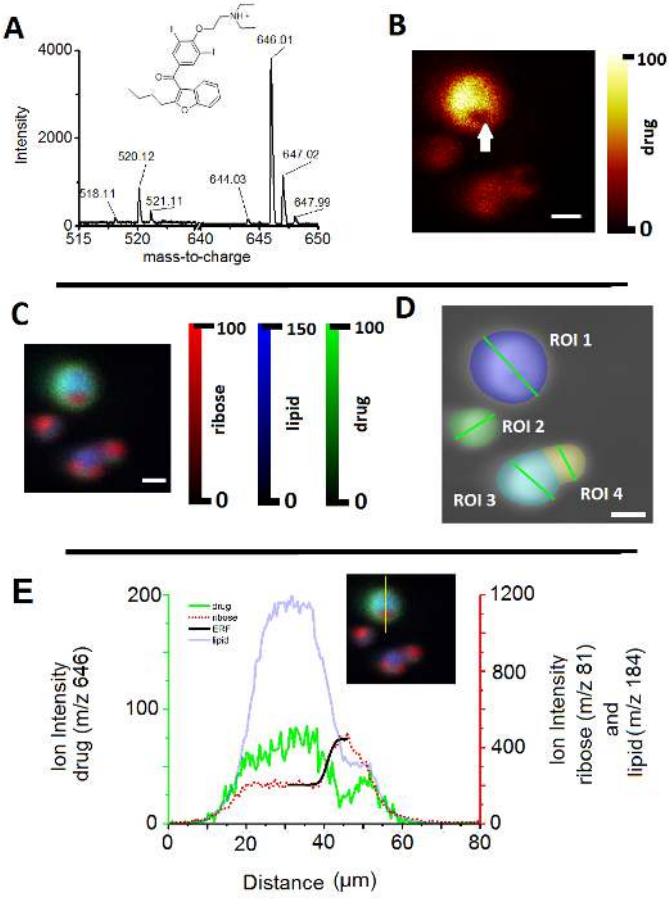

Figure 1: A) Regions of the mass spectrum obtained from a single cell showing the drug-related peaks, including the protonated molecule at m/z 646.0 and fragment ion at m/z 520.1. The molecular structure of the pharmaceutical compound amiodarone is also shown. B) The ion image of amiodarone summed over the entire depth range shows the distribution of drug compound within individual cells. C) Overlaid ion image reveals the distribution of ribose (red), lipid (blue), and drug (green) in cultured cells. D) Four regions of interest were defined on the total ion image and the diameters of the individual cells were measured. E) Linescan of the ion intensities of phosphocholine fragment (m/z 184), ribose fragment (m/z 81) and amiodarone (m/z 646) across the large cell in ROI 1 (linewidth = 3 image pixels, ion intensity summed across the depth scale). The linescan shows a reduced drug and lipid signal in the region with high ribose signal intensities. The intracellular interface between the ribose and drug signal was fitted with a error function (erf). The lateral resolution was measured to 3.4 μm. [all scale bars = 20 μm]

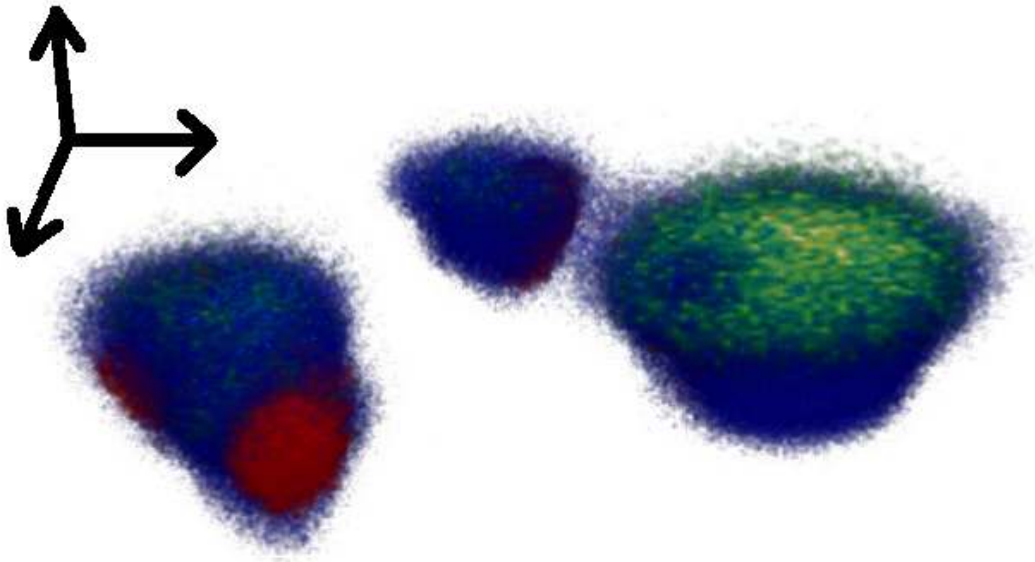

Figure 2: A) 3D rendering of macrophages dosed with amiodarone. The internal distribution of amiodarone (m/z 646.0, green) is visible after the surface of the cells was sputtered away (1.85 x 10^{14} Ar_{2000}/cm^2, slice 5-40). The blue and red pixels represent the distribution of the lipid markers at m/z 184.1 and the nuclear-markers at m/z 81.0, respectively. Note: The image is not corrected for topography.

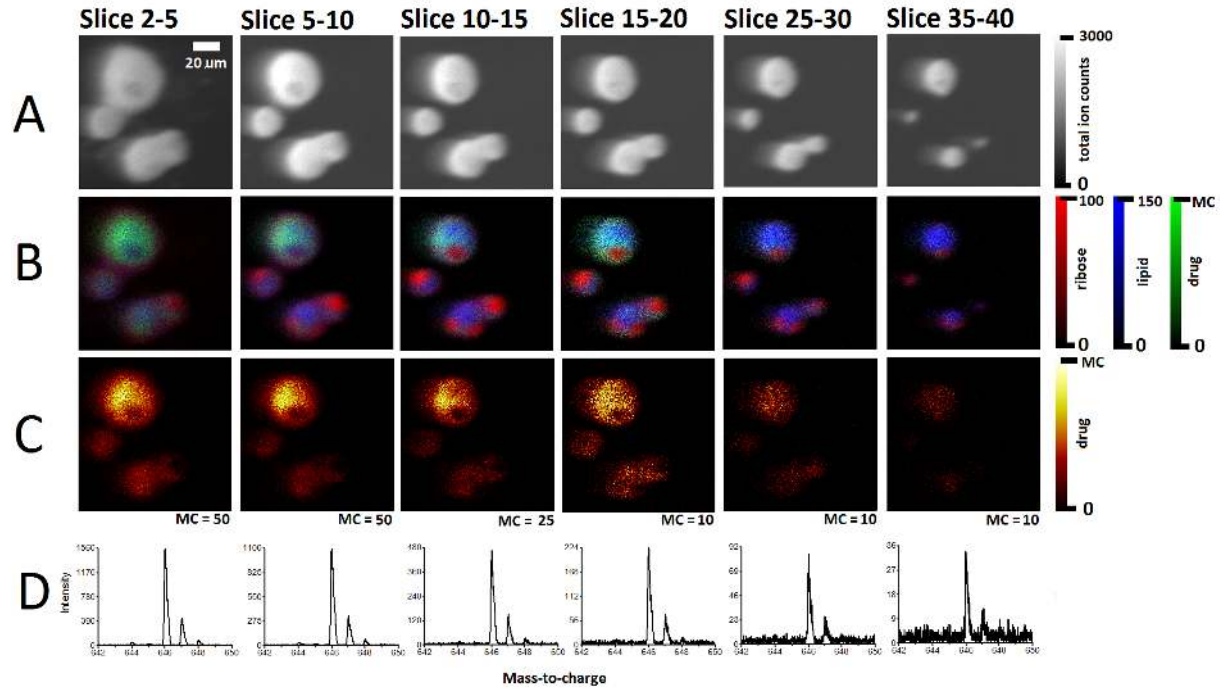

Figure 3: A) The total ion SIMS images of the amiodarone-doped macrophages at various sputter depths (maximum count 3000). B) Endogenous chemical signals for lipid markers (blue) at m/z 184.1 and nuclear-markers (red) at m/z 81.0 provide sub-cellular markers for the relative distribution of the drug, amiodarone (green). C) The protonated amiodarone molecular ion image shows the cellular distribution of the drug compound D) Mass spectra showing the relative signal-to-noise of the amiodarone peak at m/z 646.0 as a function of depth.

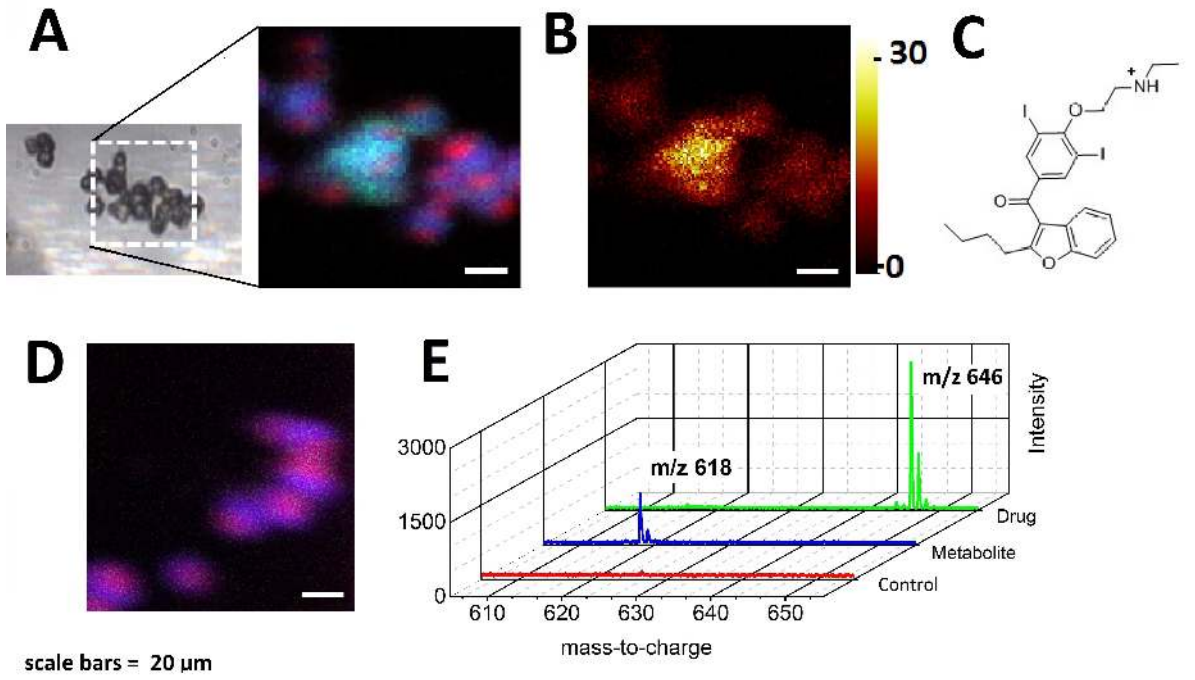

Figure 4: A) The optical and RGB ion image showing the relative distribution of lipids (blue), nuclear-markers (red) and amiodarone metabolite, desethylamiodarone (green) in macrophages. B) The total ion contribution of the protonated molecule peak for desthylamiodarone at m/z 618.0. C) The molecular structure of the drug-metabolite, desethylamiodarone. The drug molecule loses a ethyl group from the nitrogen atom when it is metabolized in the liver. D) The RGB ion image of control cells with lipid-markers (blue) and nuclear-markers (red). E) Mass spectra from cell doped with amiodarone (green) and metabolite (blue), as well as, control cells (red). [All scale bars = 20 μm]

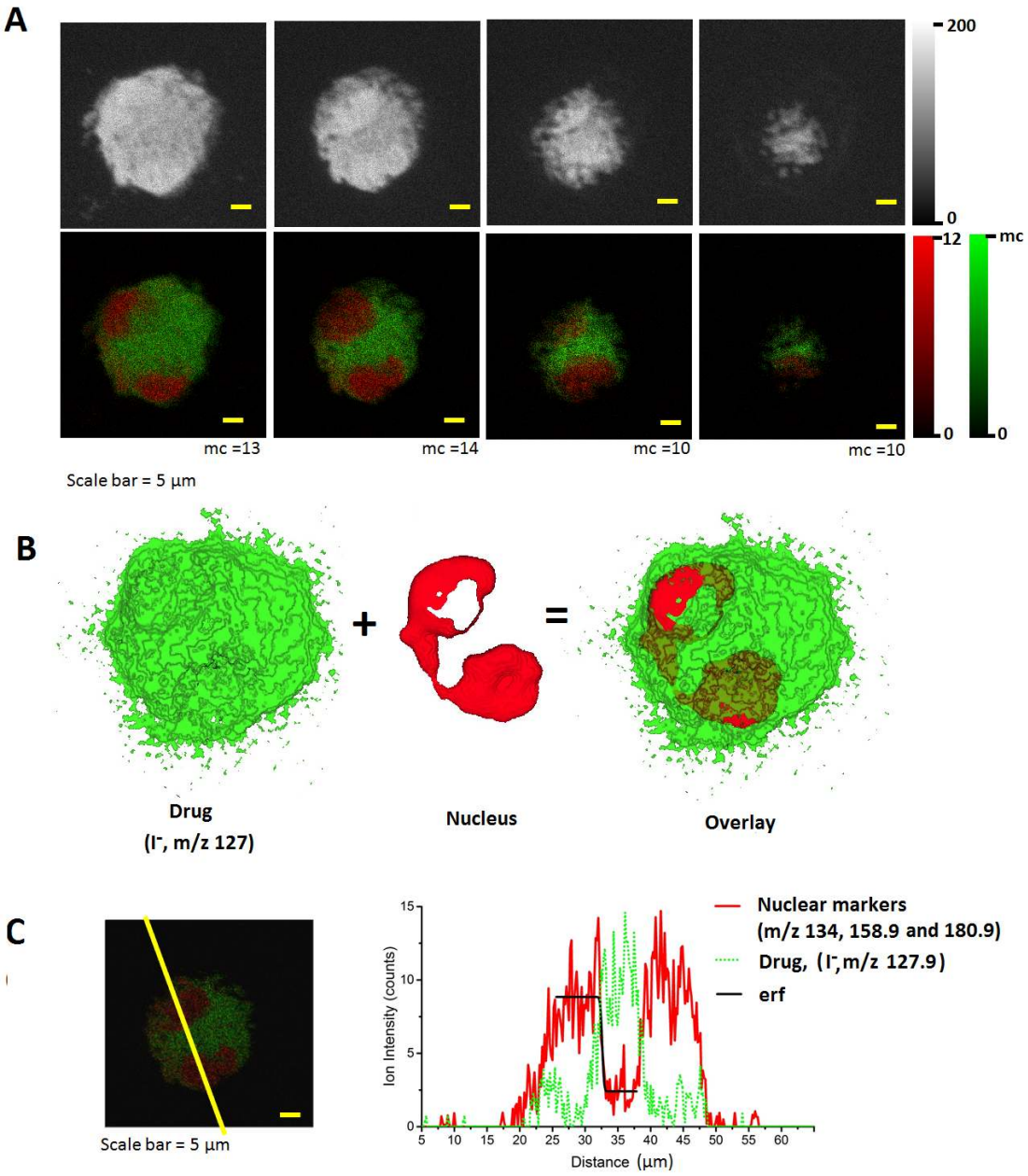

Figure 5: A) High lateral resolution ion images of NR8383 macrophage doped with desethylamiodarone in the negative ion mode at 7.8 x 10^{13} ions/cm^2, 1.56 x 10^{14} ions/cm^2, 2.34 x 10^{14} ions/cm^2, and 3.12 x 10^{14} ions/cm^2 [row 1 = total ion images, row 2 = I^- at m/z 127 (green) and the summed ion contribution of the nuclear-markers at m/z 134, 158.9 and 180.9 (red)] B) 3D isosurface rendering of the doped cell. Iodine, I^-, at m/z 127 is mapped in green (opacity = 0.65) and nuclear marker, $HP_2O_6^-$, at m/z 158.9 is mapped in red. [isosurface parameters: iso value = 16, median kernel size = 4, images were smoothed with a gauss followed by a median filter.] C) Linescan (line width = 3 image pixels) across the high lateral resolution ion image obtained after an argon sputter dose of 1.95 x 10^{14} ion/cm^2 (green = I^- signal at m/z 127 and red = summed signal from nuclear markers at m/z 134, 158.9 and 180.9) shows a reduced drug signal in the region with intense nucleus-related signals. The intracellular interface between the nucleus and drug signal was fitted with a error function (erf, black) and the lateral resolution was measured to 550 nm.